Marine tephrochronology of the Mt. Edgecumbe Volcanic Field, Southeast Alaska, USA

Jason A. Addison [a,b,*], James E. Beget [a,b], Thomas A. Ager [c], Bruce P. Finney [d]

[a] Alaska Quaternary Center and Department of Geology and Geophysics, University of Alaska Fairbanks, 900 Yukon Drive, PO Box 755780, Fairbanks, AK 99775-5780, USA
[b] Alaska Quaternary Center, PO Box 755940, University of Alaska Fairbanks, Fairbanks, AK 99775-5940, USA
[c] U.S. Geological Survey, Mail Stop 980, Box 25045, Denver Federal Center, Denver, CO 80225, USA
[d] Department of Biological Sciences, Idaho State University, Pocatello, ID 83209-8007, USA

ABSTRACT

The Mt. Edgecumbe Volcanic Field (MEVF), located on Kruzof Island near Sitka Sound in southeast Alaska, experienced a large multiple-stage eruption during the last glacial maximum (LGM)–Holocene transition that generated a regionally extensive series of compositionally similar rhyolite tephra horizons and a single well-dated dacite (MEd) tephra. Marine sediment cores collected from adjacent basins to the MEVF contain both tephra-fall and pyroclastic flow deposits that consist primarily of rhyolitic tephra and a minor dacitic tephra unit. The recovered dacite tephra correlates with the MEd tephra, whereas many of the rhyolitic tephras correlate with published MEVF rhyolites. Correlations were based on age constraints and major oxide compositions of glass shards. In addition to LGM–Holocene macroscopic tephra units, four marine cryptotephras were also identified. Three of these units appear to be derived from mid-Holocene MEVF activity, while the youngest cryptotephra corresponds well with the White River Ash eruption at ~1147 cal yr BP. Furthermore, the sedimentology of the Sitka Sound marine core EW0408-40JC and high-resolution SWATH bathymetry both suggest that extensive pyroclastic flow deposits associated with the activity that generated the MEd tephra underlie Sitka Sound, and that any future MEVF activity may pose significant risk to local population centers.

© 2009 University of Washington. Published by Elsevier Inc. All rights reserved.

Introduction

Tephrochronology has long been recognized as an important tool for establishing regional correlations and constraining chronostratigraphic units in terrestrial areas that have extensive historic and prehistoric volcanism. Recent studies have also begun to utilize tephrochronology to correlate between terrestrial and marine sedimentary records in an effort to develop more complete and comprehensive chronologies of regional geologic change (Stoner et al., 2007; Hillenbrand et al., 2008). Tephra correlations can provide precise tie points between widely separated terrestrial and marine proxy climate records, and can also be used to determine the reservoir age-correction factor for marine radiocarbon samples, thus providing an additional tool to constrain marine sediment core chronologies for calculating age–depth models (Sikes et al., 2000). The recognition of cryptotephra deposits has added further value to tephrochronological studies because of the prevalence of these units in several types of marine and terrestrial sedimentary sequences (Turney et al., 1997; Davies et al., 2005), with cryptotephras typically comprised of fine volcanic glass shards (<100-μm diameter)

sparsely preserved and/or invisible within peat, lacustrine, marine, or ice core archives (Lowe, 2008).

This study reports on the marine tephrochronologic record of southeastern Alaska using a suite of sediment piston cores recovered by the R/V Maurice Ewing in 2004. Tephra samples were geochemically analyzed to constrain these sediment cores chronologically, as well as to develop marine–terrestrial correlations for these fallout deposits. This article is the first study of coastal marine–terrestrial tephra correlations in the Subarctic Northeast Pacific Ocean.

Geologic setting

Quaternary volcanism in southeast Alaska is dominated by the regionally extensive volcaniclastic deposits of the Mt. Edgecumbe Volcanic Field (MEVF), located on the southern end of Kruzof Island near Sitka Sound (Fig. 1; Grewingk, 1850). The MEVF is composed of two eruptive centers arranged along a northeast–southwest axis and has had intermittent activity since 611 ± 74 ka (Riehle et al., 1989) with its most recent eruption between 4260 and 4820 calibrated yr before present (cal yr BP; Riehle and Brew, 1984). Bathymetric surveys of the adjacent Kruzof Island shelf have also revealed an additional extensive submarine volcanic field that was exposed during the sea level lowstand associated with the last glacial

* Corresponding author. 308 Reichardt Building, AK 99775-5780, USA.
E-mail addresses: jaaddison@alaska.edu (J.A. Addison), ftjeb1@uaf.edu (J.E. Beget), tager@usgs.gov (T.A. Ager), finney@isu.edu (B.P. Finney).
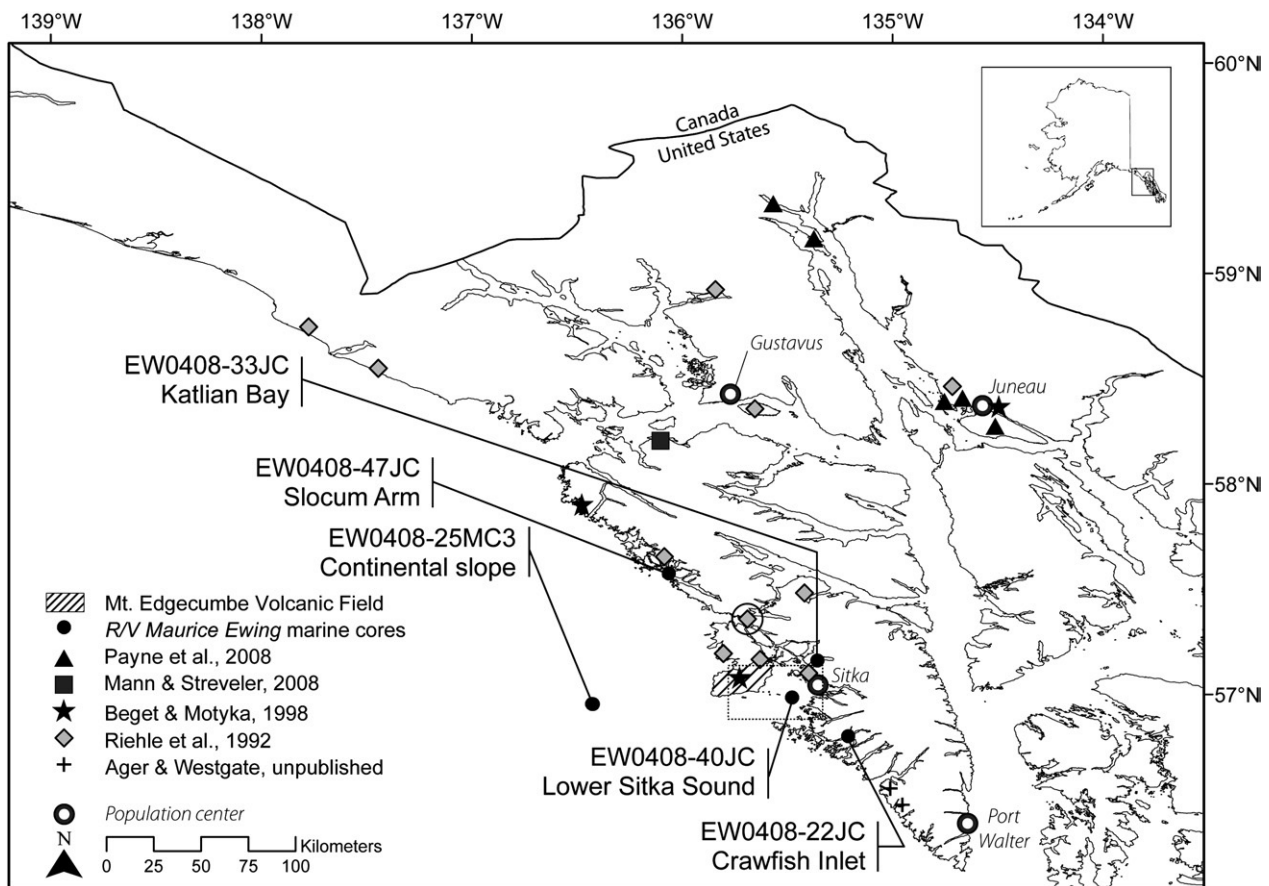
Figure 1. Location map of R/V *Maurice Ewing* marine sediment cores discussed in this study, as well as outcrops of MEVF-derived tephras previously described. Encircled diamond indicates location of lake core described in text (Riehle et al., 1992b). Dashed inset represents extent of Figure 9.

maximum (LGM) and perhaps other glacial stadia (Greene et al., 2007).

Volcaniclastic deposits from the MEVF range in composition from basalt to rhyolite (Fig. 2) and reflect a stratified magma chamber source (Riehle et al., 1992a). Early eruptive products were dominated by basalt, basaltic andesite, and andesite; activity then transitioned to more silicic material that resulted in several extensive Latest Pleistocene and early Holocene tephra-fall deposits (Riehle et al., 1992b; Beget and Motyka, 1998). Of these silicic deposits, a single dacite unit MEd has been correlated regionally and well-dated to between 13,050–13,250 cal yr BP (Beget and Motyka, 1998).

The southeast Alaska margin has also experienced limited volcanism unrelated to the MEVF. Several small vents have generated small effusive basalt flows, but no major intermediate or silicic eruptive units unrelated to activity at MEVF have been observed (Eberlein and Churkin, 1970). A recent survey of terrestrial peat bogs near the Juneau area found several cryptotephra deposits (Payne and Blackford, 2004; Payne et al., 2008), although surprisingly, none of these tephras share a geochemical affinity with published data on MEVF deposits. Payne et al. (2008) recognized a consistent 'Lena tephra' common among the five peat cores they analyzed. Although this Lena tephra was geochemically correlative with the White River Ash (WRA) deposit (Downes, 1985; Beget et al., 1992; Richter et al., 1995), two accelerator mass spectrometry (AMS) radiocarbon dates underlying the deposit in one peat core gave an age range of 280–460 cal yr BP (equivalent to AD 1670–1490), making the Lena tephra 500 yr younger than the extensive and well-documented WRA. In addition, Payne et al. (2008) also discovered evidence of (i) a single tephra layer at 1260–1375 cal yr BP, identical to the WRA as dated by Clague et al. (1995); (ii) a previously unidentified Aniakchak eruption

that occurred between 5030–5300 cal yr BP; and (iii) a second WRA-like tephra at ~6330 cal yr BP.

Methods

The R/V *Maurice Ewing* collected a suite of short multicores, trigger cores, and jumbo piston cores (10-cm diameter and up to 18-m length) along the continental shelf of southeast and southcentral Alaska in 2004. A suite of geophysical measurements was performed on each core using a ship-borne GEOTEK Multi-Sensor Core Logger, including continuous 1-cm-resolution measurements of both gamma-ray wet bulk density and volume magnetic susceptibility. Following geophysical analysis, each core was subsequently split, the sedimentary lithologies were described, and high-resolution linescan images were recorded.

Nine tephras were visually identified in core EW0408-40JC (Fig. 3A), as well as an additional macroscopic tephra in EW0408-25MC3. While tephras tend to have both higher density and magnetic susceptibility values relative to biogenic-rich sediments (Beget et al., 1994; Haberle and Lumley, 1998; Lowe, 2008), several of the EW0408-40JC tephras do not exhibit such geophysical properties, possibly as a result of either low iron concentrations or inaccuracies due to the bulk whole-core measurements. Nevertheless, the volcanic nature of these identified units was confirmed by optical smear slide analysis and subsequent geochemical analysis as described below. Combined volume magnetic susceptibility measurements and smear slide analysis also revealed the presence of two additional cryptotephras in EW0408-33JC, and one cryptotephra each in cores EW0408-22JC and -47JC (Fig. 3B).

Approximately 20 cm^3 of material was collected from each tephra sample. The four cryptotephra samples were concentrated
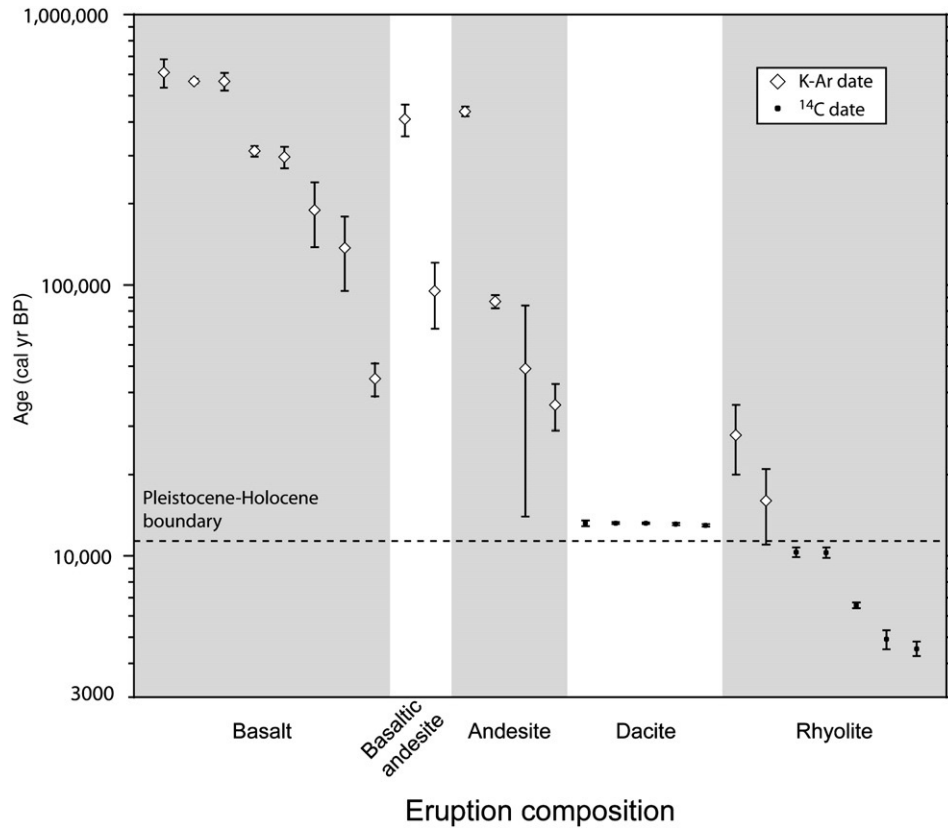
Figure 2. Quaternary history of terrestrial volcanic tephra deposits from the MEVF. Dates and geochemical compositions are based on data compiled from Riehle and Brew (1984), Riehle et al. (1992a), Riehle et al. (1992b), and Beget and Motyka (1998). All ^{14}C dates have been calibrated to calendar years BP using the CALIB 5.01 program (Stuiver and Reimer, 1993) and the INTCAL04 curve (Reimer et al., 2004).

using the sodium polytungstate density separation technique outlined by Blockley et al. (2005), with minor modifications including the use of a weaker 5% HCl acid wash and targeted sieving for tephra-rich size fractions in bulk sediment splits. Samples were dried at 50°C for several days to drive off moisture, and thin sections were prepared for each sample. Tephra grains were set in a matrix of Petro-Poxy, and the surface was polished to a smoothness of <1 μm. Following the application of a 300-Å-thick carbon coating, samples were analyzed for major elemental compositions using grain-specific electron probe microanalysis (EPMA) on a Cameca SX-50 microprobe with four wavelength-dispersive spectrometers at the University of Alaska Advanced Instrumentation Laboratory. Beam conditions were set to an accelerating voltage of 15 keV at 10 nA current with a beam diameter of 10 μm. A minimum of forty glass grains per sample were analyzed to minimize intra-sample variations. Replicate samples of the well-characterized Old Crow tephra (Beget and Keskinen, 2003) were also analyzed to monitor inter-run accuracy and instrument drift during EPMA analysis. Inaccurate grain analyses were removed from each sample dataset based on the following qualifiers: (i) obvious non-tephra geochemistry (e.g., feldspar, quartz, olivine, etc.); (ii) calculated H$_2$O content >10 wt.% (Pollard et al., 2006; Pearce et al., 2008); (iii) any elemental concentration below EPMA detection limits; and (iv) single outliers in discernible grain populations. While discarding single grains may inadvertently remove subpopulations from the larger sample dataset, these single grains may represent magma heterogeneities (Downes, 1985; Riehle et al., 2008; Shane et al., 2008), volatilization of mobile elements during EPMA analysis (Goldstein et al., 2003), or alternatively potential contamination by reworked tephra from earlier eruptive activity. Given that tephra glass is an ubiquitous background component of Gulf of Alaska

sediment (Shipboard Science Party, 1993) and the large number of explosive eruption events along the Alaskan coastline throughout the Quaternary Period (e.g., Miller and Smith, 1987; Riehle et al., 1999; Fierstein, 2007), this conservative approach seems appropriate to distinguish primary tephra-fall events from post-eruptive sedimentary mixing.

Tephra-derived glass samples were classified according to the International Union of Geological Sciences total alkali–silica classifications of Le Bas et al. (1986) after normalizing analytical totals to 100 wt.% on a volatile-free basis. Correlations to published MEVF tephra glass deposits were made using the datasets of Riehle and Brew (1984), Riehle et al. (1992a), Riehle et al. (1992b), Beget and Motyka (1998), and unpublished datasets provided by J. Riehle and J. Westgate. Correlation coefficients between samples were calculated using the standard-deviation-weighted multivariate SIMAN analysis of Borchardt et al. (1972) and Borchardt (1974). This statistical approach derives a similarity coefficient d between tephra sets A and B such that

$$d_{(A,B))} = \frac{\sum\limits_{i=1}^{n} R_i g_i}{\sum\limits_{i=1}^{n} g_i} \tag{1}$$

where R is the ratio between a mean oxide concentration $(\bar{X})$ from A and B where

$$R_i = \frac{\bar{X}_{iA}}{\bar{X}_{iB}} \text{ if } \bar{X}_{iB} > \bar{X}_{iA} \text{ or } R_i = \frac{\bar{X}_{iB}}{\bar{X}_{iA}} \text{ if } \bar{X}_{iA} > \bar{X}_{iB} \tag{2}$$
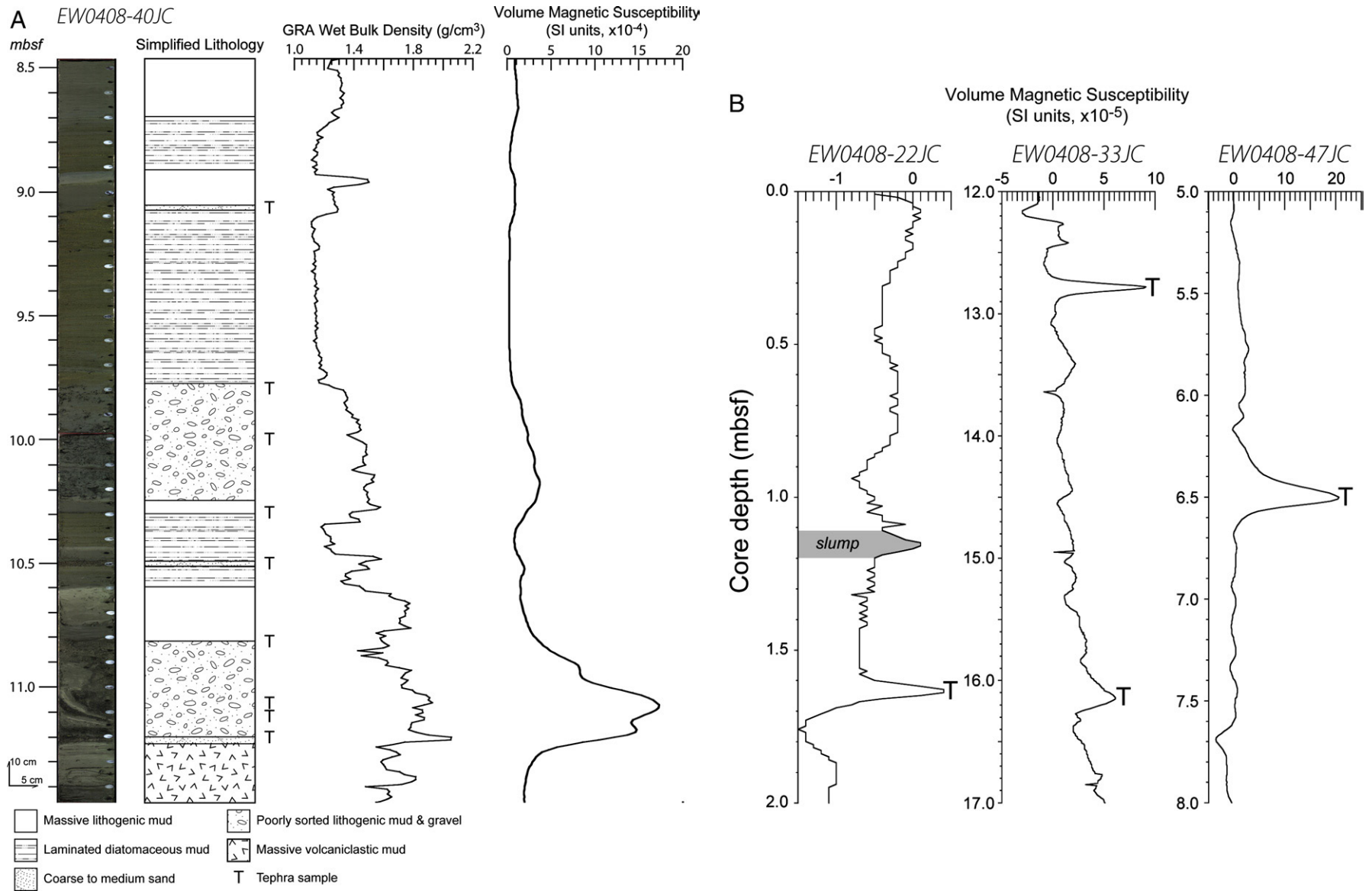
Figure 3. (A) High-resolution linescan imagery, simplified lithology, tephra sample positions, and GEOTEK geophysical measurements from core EW0408-40JC. (B) Volume magnetic susceptibility logs used to assist with identification of crytotephras in cores EW0408-22JC, -33JC, and -47JC; tephra presence was confirmed using smear slide light microscopy.

Eq. (1) also includes a weighting term g that is derived from the relationship between the standard deviation (σ) and mean of an oxide analysis by means of the relative analytical deviation function RD

$$g_i = 1 - \frac{RD_i}{ERLEV} \tag{3}$$

$$RD_i = \sqrt{\left(\frac{\sigma_{iA}}{\overline{X}_{iA}}\right)^2 + \left(\frac{\sigma_{iB}}{\overline{X}_{iB}}\right)^2} \tag{4}$$

The ERLEV function is the relative analytical deviation corresponding to the instrumental detection limits and is assigned a value between 0 and 1 by the investigator. It has the practical effect of minimizing the weighting of a particular oxide that may have a large uncertainty associated with its measurement as determined by the standard deviation from the mean. This weighted SIMAN approach differs from its traditional application in tephra similarity analyses (e.g., Beget et al., 1992; Payne et al., 2008). In this article, ERLEV was intentionally minimized on a sample-by-sample basis such that the oxides with the largest standard deviations were excluded from the similarity calculations. For a mean ERLEV value of 0.85, this approach usually removed TiO_2, and occasionally Cl, from the similarity calculations. The accuracy of the SIMAN analysis was verified using oxide bivariate and ternary plots.

Geochronology

A core chronology was developed for EW0408-40JC using AMS radiocarbon dates on five marine bivalves (Table 1; Fig. 4). Calibrations to calendar years BP were calculated according to the INTCAL04 curve (Reimer et al., 2004), using the CALIB 5.01 software of Stuiver and Reimer (1993), assuming a carbon reservoir effect of 732 yr, based on the mean ^{14}C date discrepancy between paired marine bivalve and terrestrial wood samples from three different EW0408 coastal marine sediment cores. A linear interpolated depth–age model ($r^2 = 0.98$) was then used to convert depths in EW0408-40JC into ages.

The EW0408-22JC cryptotephra at 1.63 m below seafloor (mbsf) is constrained by two AMS-radiocarbon-dated wood fragments, while an additional AMS sample at 0.98 mbsf was rejected due to an apparent age reversal (Table 1). The stratigraphic order and lack of overlap between the uncalibrated ^{14}C dates of the two accepted AMS

samples argue against deposition of reworked organic material. The 2σ INTCAL04 calibration ranges of the two AMS samples overlap, indicating a period of rapid sediment accumulation during this interval. Applying a linear interpolation between these two samples and assuming steady-state sediment accumulation gives an age for the EW0408-22JC cryptotephra of ~1200 cal yr BP. An ^{137}Cs- and excess ^{210}Pb-supported chronology developed for the corresponding gravity core EW0408-21GC yields a maximum apparent sedimentation rate of between 3 and 4 mm/yr (Jaeger, J.M. and Rosen, G.P., personal communication, 2007), in broad agreement with the interpolated calibrated ^{14}C age. Given the limited geochronological constraints in this interpolation, the age of deposition of the cryptotephra should be considered a first-order approximation.

Four AMS ^{14}C dated wood fossils constrain the two cryptotephas within core EW0408-33JC (Table 1). These four samples are part of a larger AMS dataset that chronologically constrains the full length of EW0408-33JC (Fig. 4); the full description of these data is beyond the scope of this current work. The full model yields a linear interpolated age for the upper tephra at 12.78 mbsf of ~5300 cal yr BP, whereas the lower cryptotephra at 16.18 mbsf is calculated to be ~6750 cal yr BP.

The cryptotephra deposit at 6.46 mbsf recovered in core EW0408-47JC lies above three AMS ^{14}C samples of terrestrial wood fragments (Fig. 4). The closest radiocarbon date to the tephra is between 7501 and 7608 cal yr BP at 7.28 mbsf (Table 1). A linear depth–age model constructed using this AMS sample and the two lower samples deeper in core EW0408-47JC give an extrapolated age for the tephra of ~7300 cal yr BP.

Because of the prevalence of bioturbation along the Gulf of Alaska continental slope, the visible macroscopic tephra in core EW0408-25MC3 at 0.21 mbsf remains undated at this time. It lies below the 11-cm-thick surface mixed layer, as evidenced by the maximum depth of excess ^{210}Pb, so it is a minimum of 100 yr old (Rosen et al., 2005; Walinsky et al., 2009). Rosen et al. hypothesize that the relatively high levels of bioturbation in this core are a consequence of a reduced continental shelf accumulation rate due to sediment entrapment by adjacent nearshore embayments.

Results

Fourteen tephras were geochemically analyzed by EPMA (Table 2). Two coherent subpopulations were also found in samples 9.08 mbsf

Table 1
AMS ^{14}C dates constraining EW0408 tephras.

Core depth (mbsf)	Material	Reported ^{14}C age (^{14}Cyr BP)	Corrected ^{14}C age (^{14}Cyr BP)[a]	2σ Calibrated range (cal yr BP)	AMS ^{14}C laboratory[b]	Sample ID
EW0408-22JC						
0.82	terrestrial organics	1240 ± 20		1083–1263	Keck–UCI	65,503
0.98	terrestrial organics[c]	1505 ± 20		1336–1480	Keck–UCI	50,810
2.17	wood fragment	1335 ± 20		1185–1300	Keck–UCI	50,811
EW0408-33JC						
10.99	terrestrial organics	3980 ± 20		4416–4517	Keck–UCI	50,818
13.94	wood fragment	4985 ± 30		5619–5878	CAMS–LLNL	127,768
16.00	terrestrial organics	5880 ± 20		6659–6743	Keck–UCI	50,819
17.03	wood fragment	6485 ± 20		7327–7434	Keck–UCI	50,820
EW0408-40JC						
0.96	bivalve	$10,881 \pm 61$	$10,149 \pm 61$	11,408–12,054	NSF–AAMS	WW5472
1.89	bivalve	$10,952 \pm 55$	$10,220 \pm 55$	11,713–12,142	NSF–AAMS	WW5473
3.75	bivalve	$10,987 \pm 56$	$10,255 \pm 56$	11,759–12,348	NSF–AAMS	WW5474
5.94	bivalve	$11,126 \pm 59$	$10,394 \pm 59$	12,055–12,605	NSF–AAMS	WW5475
8.61	bivalve	$11,522 \pm 58$	$10,790 \pm 58$	12,725–12,885	NSF–AAMS	WW5476
EW0408-47						
7.28	wood	6685 ± 30		7501–7608	NSF–AAMS	WW6079
11.28	wood	7660 ± 30		8398–8538	NSF–AAMS	WW6080
17.80	wood	8865 ± 50		9744–10,176	NSF–AAMS	WW6104

[a] Marine reservoir correction of 732 yrs subtracted from carbonate samples.

[b] Keck–UCI = Keck Carbon Cycle AMS facility, University of California–Irvine; CAMS–LLNL = Center for Accelerator Mass Spectrometry, Lawrence Livermore National Lab; NSF–AAMS = National Science Foundation–Arizona AMS facility, Tucson.

[c] Sample rejected from age model; see text for details.
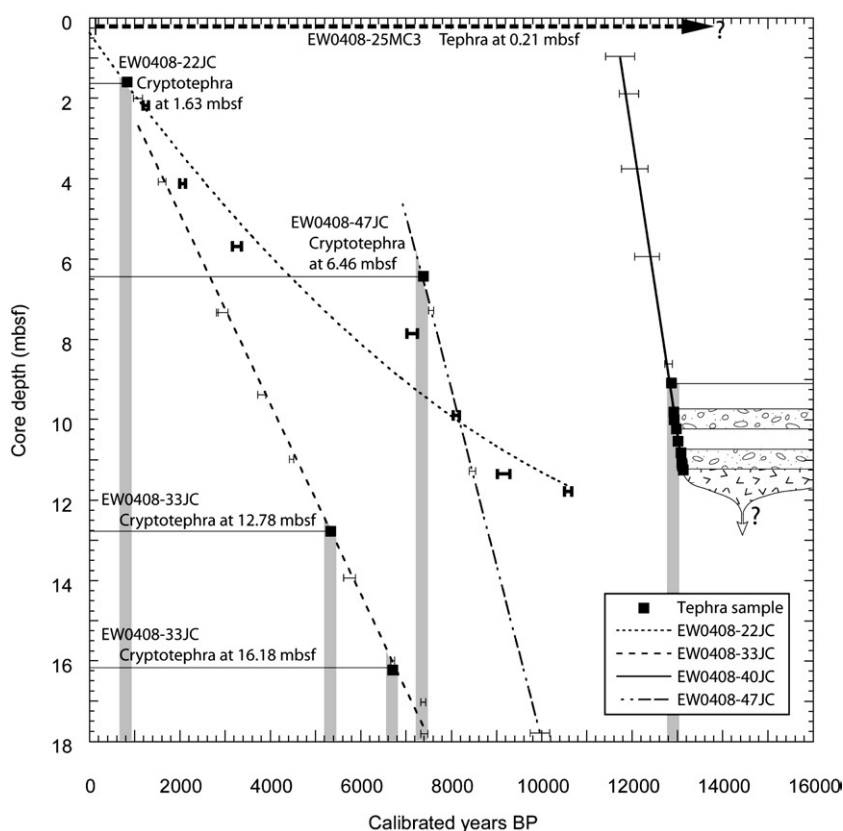
Figure 4. Depth–age relationships for EW0408 tephra-bearing marine sediment cores discussed in the text. Error bars represent the 2σ calibration range for dated AMS samples. Bold error bars correspond to EW0408-22JC age model. Because of poor age control, the EW0408-25MC3 tephra is only constrained beyond the depth of excess ^{210}Pb (>100 yr BP; Rosen et al., 2005; Walinsky et al., 2009). Depths of gravity and pyroclastic flow deposits are indicated for EW0408-40JC; lithologies are the same as in Figure 3. Thickness of basal EW0408-40JC pyroclastic deposit is unknown.

and 6.46 mbsf in cores EW0408-40JC and -47JC, respectively. These subpopulations were identified on the basis of (i) distinctive differences in geochemistry from the primary population and (ii) several glass particles shared this same composition. For the purposes of discussion in this text, the primary populations are indicated by the (I) designation, while the secondary populations are marked by a (II)

Table 2
Mean glass EPMA analyses of EW0408 tephra samples.

	n	Na$_2$O	MgO	Al$_2$O$_3$	SiO$_2$	Cl	K$_2$O	CaO	TiO$_2$	Fe$_T$O$_3$	H$_2$O
Old Crow Tephra											
internal standard	194	3.80 ± 0.30	0.30 ± 0.03	13.24 ± 0.20	75.05 ± 0.38	0.29 ± 0.06	3.72 ± 0.23	1.45 ± 0.10	0.30 ± 0.17	1.85 ± 0.15	5.10 ± 2.07
EW0408-22JC: Crawfish Inlet											
1.63 mbsf	11	4.17 ± 0.36	0.32 ± 0.09	14.63 ± 0.08	73.28 ± 0.33	0.19 ± 0.15	2.93 ± 0.41	1.89 ± 0.10	0.28 ± 0.14	2.32 ± 0.51	4.41 ± 2.48
EW0408-25MC3: Sitka Slope											
0.21 mbsf	20	4.49 ± 0.16	0.31 ± 0.04	14.05 ± 0.35	73.34 ± 0.50	0.15 ± 0.10	2.61 ± 0.09	1.86 ± 0.17	0.26 ± 0.16	2.92 ± 0.15	1.36 ± 2.23
EW0408-33JC: Katlian Bay											
12.78 mbsf	13	4.58 ± 0.13	0.29 ± 0.05	14.72 ± 0.35	72.95 ± 0.40	0.09 ± 0.03	2.58 ± 0.15	1.89 ± 0.17	0.17 ± 0.09	2.74 ± 0.17	2.77 ± 1.57
16.18 mbsf	19	5.02 ± 0.19	0.28 ± 0.06	14.35 ± 0.38	72.97 ± 0.58	0.09 ± 0.03	2.52 ± 0.19	1.64 ± 0.25	0.33 ± 0.12	2.81 ± 0.21	3.80 ± 2.71
EW0408-40JC: Lower Sitka Sound											
9.08 mbsf (I)	21	5.01 ± 0.33	0.31 ± 0.13	14.58 ± 0.28	72.50 ± 0.55	0.08 ± 0.03	2.56 ± 0.15	1.73 ± 0.12	0.33 ± 0.10	2.90 ± 0.30	4.55 ± 1.30
9.08 mbsf (II)	7	5.03 ± 0.37	0.58 ± 0.43	14.77 ± 0.78	71.27 ± 0.52	0.09 ± 0.01	2.36 ± 0.19	1.95 ± 0.22	0.57 ± 0.21	3.37 ± 0.91	3.35 ± 1.50
9.80 mbsf	14	5.36 ± 0.61	0.28 ± 0.04	14.53 ± 0.17	72.93 ± 0.50	0.08 ± 0.03	2.20 ± 0.13	1.45 ± 0.19	0.31 ± 0.12	2.85 ± 0.18	1.71 ± 1.59
10.00 mbsf	10	5.82 ± 0.35	0.29 ± 0.05	14.34 ± 0.30	72.88 ± 0.65	0.09 ± 0.03	2.28 ± 0.23	1.48 ± 0.23	0.22 ± 0.18	2.60 ± 0.16	4.61 ± 0.91
10.29 mbsf	58	4.75 ± 039	0.28 ± 0.05	14.65 ± 0.48	72.72 ± 0.57	0.09 ± 0.03	2.66 ± 0.18	1.76 ± 0.20	0.31 ± 0.15	2.79 ± 0.25	2.66 ± 2.05
10.49 mbsf	20	5.37 ± 0.38	0.29 ± 0.07	14.56 ± 0.38	73.01 ± 0.62	0.09 ± 0.03	2.16 ± 0.18	1.43 ± 0.20	0.30 ± 0.13	2.80 ± 0.35	1.93 ± 1.57
10.82 mbsf	27	5.43 ± 0.37	0.26 ± 0.04	14.59 ± 0.44	72.97 ± 0.74	0.08 ± 0.02	2.21 ± 0.19	1.47 ± 0.30	0.22 ± 0.17	2.76 ± 0.29	1.81 ± 1.60
11.08 mbsf	19	5.08 ± 0.18	0.30 ± 0.06	14.44 ± 0.25	72.80 ± 0.45	0.09 ± 0.04	2.48 ± 0.09	1.56 ± 0.15	0.33 ± 0.08	2.92 ± 0.21	3.27 ± 2.23
11.10 mbsf	29	5.46 ± 0.41	0.26 ± 0.06	14.53 ± 0.39	72.93 ± 0.55	0.09 ± 0.03	2.36 ± 0.17	1.44 ± 0.26	0.28 ± 0.19	2.66 ± 0.29	1.79 ± 1.14
11.20 mbsf	21	5.09 ± 0.40	0.32 ± 0.08	14.57 ± 0.29	72.37 ± 0.67	0.09 ± 0.03	2.58 ± 0.12	1.74 ± 0.17	0.32 ± 0.11	2.91 ± 0.19	4.43 ± 1.46
EW0408-47JC: Slocum Arm											
6.46 mbsf (I)	14	5.06 ± 0.25	0.30 ± 0.07	14.26 ± 0.29	72.78 ± 0.42	0.10 ± 0.04	2.57 ± 0.11	1.68 ± 0.09	0.30 ± 0.08	2.96 ± 0.23	1.74 ± 1.62
6.46 mbsf (II)	10	5.28 ± 0.17	0.70 ± 0.06	15.28 ± 0.18	69.44 ± 0.50	0.07 ± 0.04	2.04 ± 0.07	2.72 ± 0.14	0.51 ± 0.14	3.97 ± 0.21	3.77 ± 3.39

n = Total number of glass shards analyzed for each tephra sample. Mean and estimated error to one standard deviation were shown for each sample. Analyses were normalized to 100 wt.% on a water-free basis. Water content was calculated by difference from analytical total. Total iron oxide concentration was expressed as Fe$_2$O$_3$. Individual analyses are contained in an online supplement.

label. According to the Le Bas et al. (1986) classification, all samples are rhyolitic except for the dacitic secondary population in the EW0408-47JC sample at 6.46 mbsf (Fig. 5A). All geochemical analyses are included in the online data repository.

The multivariate SIMAN similarity analysis indicates four distinct rhyolitic groupings of these data (Table 3). With the exception of samples EW0408-40JC at 9.08 mbsf (II) and EW0408-22JC at 1.63 mbsf designated as Units C and D, respectively, all studied
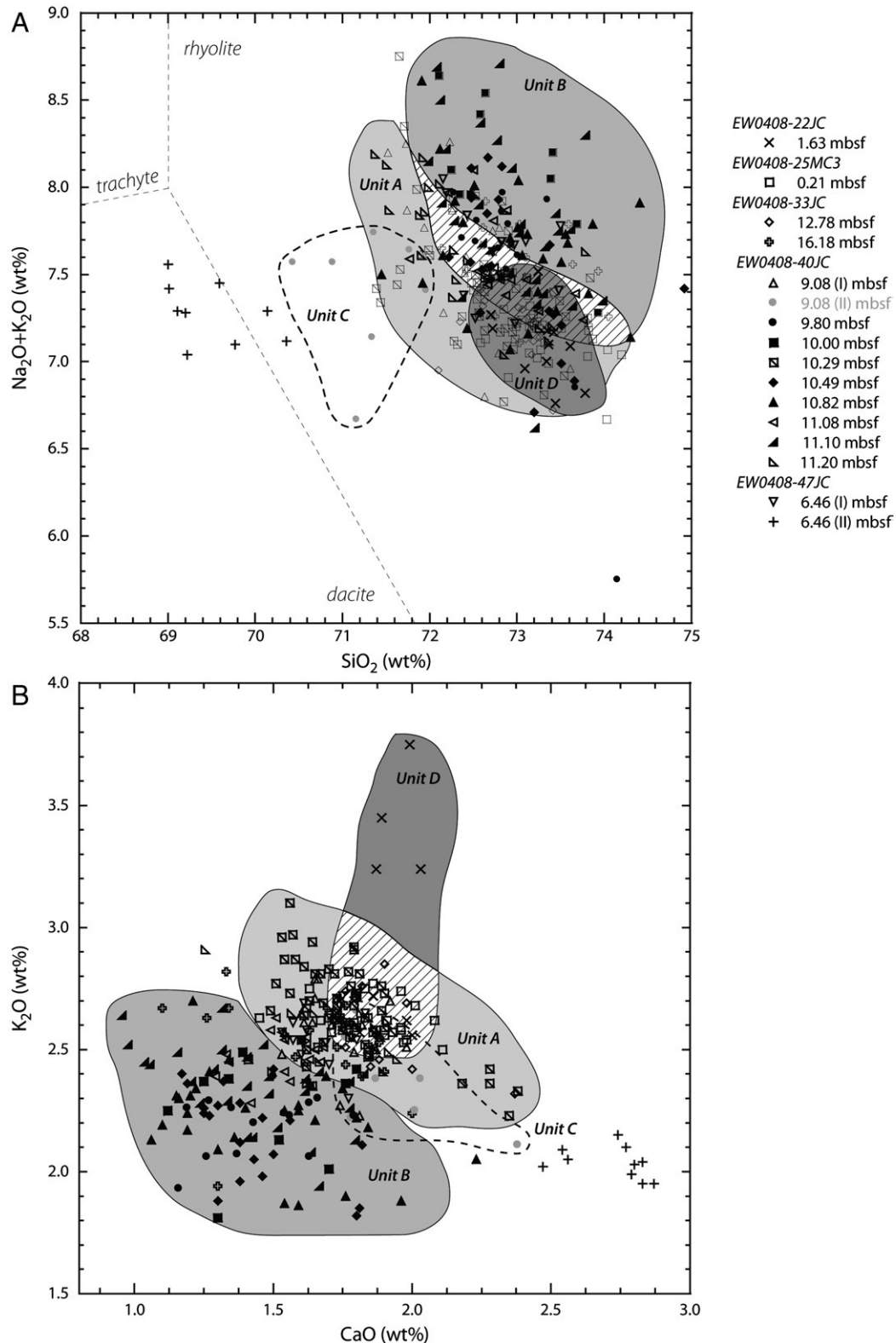
Figure 5. Total alkali–silica diagram (A) and oxide variation diagram (B) of individual EW0408 tephra glass shards. Classification based on the Le Bas et al. (1986) IUGS volcanic classification. Hollow symbols indicate geochemical affinities to SIMAN-identified Unit A; dark filled symbols represent Unit B; gray symbols represent Unit C; × symbols correspond to Unit D. Approximate compositional ranges are indicated; region of compositional overlap between Units A, B, and D is indicated by slanted lines.

tephras fall into two general categories. Unit A tephras generally contain lower concentrations of SiO_2 and total alkali, and higher Fe_2O_3 contents, than Unit B tephras. Both total alkali–silica (TAS) and CaO-K_2O variation plots agree with these generalized geochemical classifications (Fig. 5).

Discussion

Correlations: MEVF suite

The chronological and geochemical characteristics of the marine tephras described here are similar to those of several terrestrial tephras known to be part of the MEVF eruptive sequence. Applying the same SIMAN similarity analysis to previous MEVF tephra analyses yielded strong correlations (>0.95) between the Unit A tephras and several high-Si rhyolitic tephras described by Riehle et al. (1992a,b), and with an unpublished high-Si rhyolite tephra described by Westgate (Table 4). The Unit B tephras also bear some resemblance to the Riehle high-Si rhyolite (Table 4); however, the compositions appear to be distinctly different in several oxides (Fig. 6), suggesting that Unit B may be unique to this study. It is important to note that, despite the geochemical differences between Units A and B, the presence of both units in fine- and coarse-grained lithologies in core EW0408-40JC suggests the same volcanic source (e.g., the MEVF).

Unit C is composed solely of a secondary population ($n = 7$) identified in a tephra sample in core EW0408-40JC at 9.08 mbsf (II) (Tables 1 and 2). The SIMAN analysis of Unit C indicates strong affinities to several potential deposits (Table 4). However, it is the only EW0408 tephra recovered that has a relatively high similarity coefficient (>0.93) with the MEd dacite tephra of Beget and Motyka (1998). A CaO-K_2O variation plot (Fig. 6) shows considerable compositional overlap between EW0408 Unit C, the MEd dacite, and the low-Si rhyolite of Riehle et al. (1992a,b). The MEd tephra is constrained by five radiocarbon dates that, when calibrated according to the method described above, places the time of deposition of the MEd deposit between 13,050–13,250 cal yr BP (Beget and Motyka, 1998), suggesting that Unit C is broadly equivalent in age to the MEd tephra. The Late Pleistocene MEVF eruptions produced both tephra-fall and pyroclastic flow deposits with very diverse geochemical characteristics (Fig. 2; Riehle et al., 1989; Riehle et al., 1992a,b), consistent with the somewhat heterogeneous nature of sample 9.08 mbsf (II) (Fig. 6).

### Terrestrial–marine relationships with the MEVF suite

The stratigraphy of the tephra sequence in marine core EW0408-40JC resembles that of a lacustrine core (Fig. 7) recovered from an unnamed lake on Baranof Island 29 km NNE of the MEVF (Fig. 1) by Riehle et al. (1992b). The lake core (herein referred to as the Riehle

Table 3
EW0408 tephra SIMAN similarity coefficients. Results indicate four distinct geochemical similarity units are sufficient to describe full dataset. Bold values highlight SIMAN result between samples within a given geochemical similarity unit.

EW0408 core	Sample depth (mbsf)	25MC3 0.21	33JC 12.78	33JC 16.18	40JC 9.08 (I)	40JC 9.08 (II)	40JC 9.80	40JC 10.00	40JC 10.29	40JC 10.49	40JC 10.82	40JC 11.08	40JC 11.10	40JC 11.20	47JC 6.46 (I)	47JC 6.46 (II)	Geochemical similarity unit
22JC	1.63	0.94	0.93	0.89	0.91	0.87	0.86	0.87	0.93	0.86	0.86	0.89	0.86	0.91	0.90	0.77	D
25MC3	0.21	–	**0.96**	**0.94**	**0.96**	0.92	0.90	0.89	**0.95**	0.90	0.89	**0.94**	0.89	**0.96**	**0.96**	0.76	A
33JC	12.78	–	–	**0.97**	**0.95**	0.93	0.91	0.91	**0.97**	0.92	0.92	**0.94**	0.91	**0.95**	**0.95**	0.78	A
	16.18	–	–	–	**0.98**	0.91	0.95	0.96	**0.97**	0.95	0.94	**0.98**	0.94	**0.97**	**0.98**	0.79	A
40JC	9.08 (I)	–	–	–	–	0.91	0.94	0.92	**0.97**	0.93	0.93	**0.97**	0.93	**0.99**	**0.99**	0.81	A
	9.08 (II)	–	–	–	–	–	0.89	0.90	0.92	0.89	0.89	0.91	0.91	0.93	0.89	0.88	C
	9.80	–	–	–	–	–	–	**0.96**	0.94	**0.98**	**0.98**	0.95	**0.97**	0.93	0.94	0.79	B
	10.00	–	–	–	–	–	–	–	0.91	**0.96**	**0.96**	0.94	**0.97**	0.92	0.92	0.77	B
	10.29	–	–	–	–	–	–	–	–	0.93	0.93	**0.95**	0.93	**0.97**	**0.96**	0.78	A
	10.49	–	–	–	–	–	–	–	–	–	**0.98**	0.95	**0.96**	0.97	0.93	0.81	B
	10.82	–	–	–	–	–	–	–	–	–	–	0.94	**0.99**	0.92	0.92	0.79	B
	11.08	–	–	–	–	–	–	–	–	–	–	–	0.94	**0.97**	**0.98**	0.78	A
	11.10	–	–	–	–	–	–	–	–	–	–	–	–	0.93	0.92	0.79	B
	11.20	–	–	–	–	–	–	–	–	–	–	–	–	–	**0.98**	0.80	A
47JC	6.46 (I)	–	–	–	–	–	–	–	–	–	–	–	–	–	–	0.78	A

Table 4
Marine EW0408–terrestrial MEVF correlations.

EW0408 geochemistry	Unit A	Unit B	Unit C	Unit D
Representative sample	40JC–10.29 mbsf	40JC–9.80 mbsf	40JC–9.08 (II) mbsf	22JC–1.63 mbsf
Riehle high-Si dacite	0.78	0.78	0.87	0.79
Riehle low-Si rhyolite	0.87	0.87	0.94	0.85
Riehle high-Si rhyolite	**0.98**	**0.94**	0.94	0.92
Beget dacite	0.81	0.81	**0.93**	0.80
Westgate low-Si rhyolite	0.81	0.79	0.90	0.78
Westgate high-Si rhyolite	**0.96**	0.91	0.95	0.90

Bold values indicate units with high likelihood of correlation.
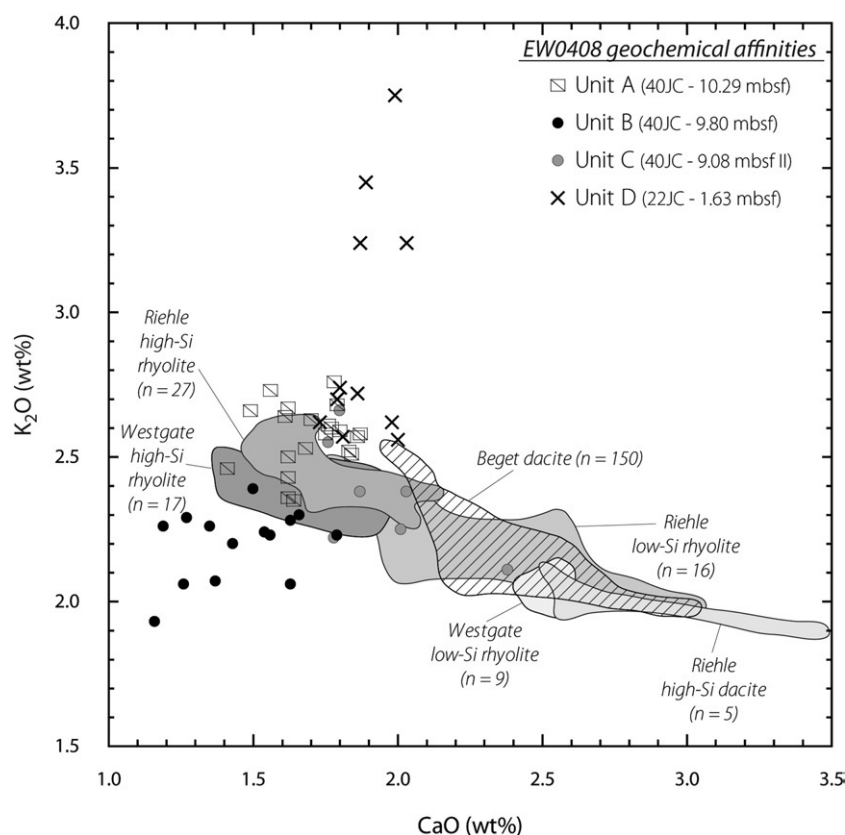
Figure 6. CaO-K$_2$O oxide variation diagram for representative EW0408 tephra geochemical units compared to previous published MEVF datasets (see text for references).

lake core) contains >0.7 m of volcanic material within lacustrine silts, and this thickness is comparable to the total thickness of volcanic material contained within EW0408-40JC after correcting for the presence of autochthonous diatom-rich muds.

We propose that the uppermost rhyolite and dacite tephra units in the Riehle lake core are correlative with the primary and secondary populations of rhyolitic tephra found in the 9.08 mbsf sample from EW0408-40JC (Fig. 7). The 9.08 mbsf samples are associated with a coarse sand that underlies a massive lithogenic mud; this fining upwards sequence suggests deposition by a fallout event into the marine environment, interrupting the deposition of in–situ diatomaceous organic matter. The lack of autochthonous organic matter in the Riehle lake core underlying the dacite may reflect (i) an erosional unconformity or hiatus between the dacite and upper rhyolite or (ii) much lower sedimentation rates, relative to the extremely high rates evident in EW0408-40JC.

The lower rhyolitic tephra in the Riehle lake core is composed of lapilli-size clasts (Riehle et al., 1992b) and is correlative with the upper poorly sorted lithogenic mud and gravel in EW0408-40JC (Fig. 7). EPMA analysis of volcanic glass from EW0408-40JC tephra samples 9.80 and 10.00 mbsf confirms a rhyolitic composition for this unit.

The andesitic tephra in the Riehle lake core does not appear in the EW0408-40JC core (Fig. 7). Given that the two cores are equidistant from the MEVF (Fig. 1), this absence suggests that the andesite deposition may have been more heavily influenced by wind direction or other processes that resulted in non-deposition.

The andesitic tephra is underlain by a mixed rhyolite/andesite unit in the Riehle lake core (Fig. 7). Although a definitive andesite population was not recognized within any of the EW0408-40JC tephra deposits, the post-EPMA data treatment of the rhyolite sample at 10.29 mbsf eliminated several glass shards. These shards represented a widely heterogeneous grouping that did not warrant classification as a separate population due to the calculated means and standard

deviations for these shards (e.g., SiO$_2$ = 65.23 ± 4.07 wt.%; n = 4). Nevertheless, the low SiO$_2$ content suggests a possible andesitic deposit within the EW0408-40JC core; further analysis is required to confirm this possibility.

The lowermost volcaniclastic unit in the Riehle lake core, a basaltic andesite, does not occur in EW0408-40JC, nor do the basal rhyolitic volcaniclastic units from EW0408-40JC appear in the Riehle lake core (Fig. 7). The divergence in sedimentology between the two cores most likely represents differences in topography related to the two coring locations. Given that Lower Sitka Sound is directly downslope from the MEVF, while a topographic high separates the Riehle lake core site from the MEVF, it follows that only fallout volcanic deposits should accumulate at the Riehle lake core location whereas both fallout and gravity-driven deposition will accumulate at the EW0408-40JC site. Thus, it seems likely that EW0408-40JC did not penetrate deep enough into the seafloor to recover the basaltic andesite observed in the Riehle lake core.

Correlations: EW0408 tephras and non-MEVF contemporaneous deposits

EW0408-22JC

The estimated age of the cryptotephra at 1.63 mbsf in core EW0408-22JC places this event at ~1200 cal yr BP. The deposition of this tephra is thus contemporaneous with the regionally extensive White River Ash deposited at ~1147 cal yr BP (Downes, 1985; Richter et al., 1995). Recent work by Robinson (2001) extends the eastern lobe of this Plinian eruption from its source near Mt. Churchill in east-central Alaska to the Great Slave Lake in Canada, with an estimated eruptive volume of approximately 47 km^3 (Lerbekmo, 2008). Furthermore, electrical conductivity spikes tied to an accumulation age model in the Prospector Ridge Col ice core from Mt. Logan are attributed to deposition of volcanic sulfate from the White River Ash eruption (Fisher et al., 2004). However, some doubt has been cast
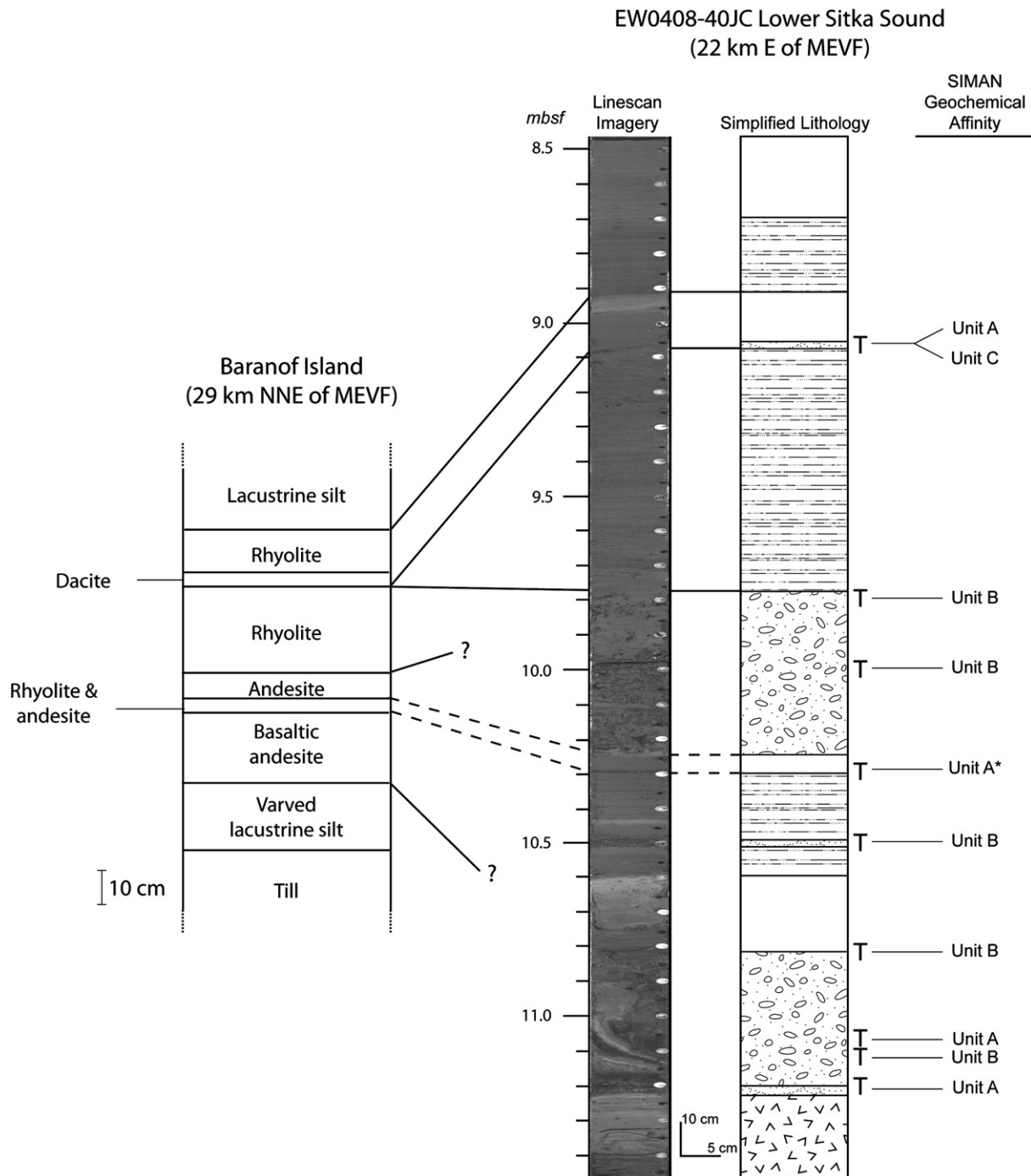
Figure 7. Correlation between published lake core from Baranoff Island (Fig. 1; Riehle et al., 1992b) and EW0408-40JC. Based on the SIMAN similarity calculation, the Unit C chemistry is analogous to the dacite unit. Asterisk (*) indicates a possible correlation; see text for explanation. Lithologies same as in Figure 3.

upon Mt. Churchill as the source of the White River Ash because of the lack of an appropriately aged deposit within an ice core collected from the col between Mts. Churchill and Bona (Mashiotta et al., 2004).

Payne et al. (2008) recovered a cryptotephra sample (LNA 100) from a peat bog near Juneau, Alaska, that is convincingly derived from the White River Ash. Payne et al. showed that their LNA 100 sample has a high geochemical similarity coefficient (>0.93), agreeing closely with previous published analyses of the White River Ash. The LNA 100 cryptotephra is also directly underlain by two fragments of *Sphagnum* moss that were AMS radiocarbon dated to 1260–1360 and 1290–1375 cal yr BP, respectively.

Applying the SIMAN similarity analysis to the published geochemistry of the White River Ash and the cryptotephra in EW0408-22JC shows that the two deposits have a similarity coefficient of 0.90 for published distal deposits and 0.89 for ash deposits recovered from the summit of Mt. Churchill proper (Table 5). However, the SIMAN analyses of both EW0408-22JC and LNA 100 of Payne et al. (2008) show a strong relationship with a similarity coefficient of 0.93. The oxide compositions of the EW0408-22JC cryptotephra and LNA 100 show a high degree of overlap (Fig. 8A). The relatively low degree of similarity calculated by the SIMAN analysis for the EW0408-22JC sample and the Mt. Churchill samples may reflect differences associated with statistical analysis (e.g., normalizations, Fe calculated as FeO or Fe_2O_3, etc.). Nevertheless, the available dates and geochemical analyses of the EW0408-22JC cryptotephra agree very well with those of the LNA 100 sample of Payne et al. (2008). Furthermore, a SIMAN analysis conducted between the EW0408-

Table 5
SIMAN similarity coefficients between EW0408 marine tephras and contemporaneous deposits. Bold values indicate likely correlation; see text for further explanation.

	EW0408-25MC3 0.21 mbsf (>50)	EW0408-22JC Unit D (1.63 mbsf) (~1200)		EW0408-33JC 12.78 mbsf (~5300)	16.18 mbsf (~6750)	EW0408-47JC 6.46 mbsf (I) (~7300)	6.46 mbsf (II) (~7300)
Mt. Katmai, Novarupta (AD 1912)[a]			Bridge River tephra (~2600)[f]				
Dacite	0.83	0.88	Otter Creek Bog[g]	0.83	0.83	0.83	0.69
Andesite	0.87	0.86					
			Aniakchak (~3400)[e]	0.87	0.89	0.88	0.82
Lena tephra, unknown source (280–320)[b]							
ECR 32	0.84	0.90	Jarvis Creek ash (~3600)[h]	0.79	0.77	0.78	0.76
Unknown source (~480)[b]			Black Peak[i] (4600–5600[1])	0.81	0.80	0.80	0.69
CHP 184	0.81	0.86					
			Unknown source (5030–5300)				
White River Ash (1147)			ECR 162[b]	**0.90**	0.89	**0.90**	0.79
Mt. Churchill summit[c]	0.83	0.89					
Distal[d,e]	0.84	**0.90**[d]	Osthena tephra (~6000)[j]	0.89	0.85	0.83	0.82
		0.94[e]					
Unknown source (1260–1375)[b]			Unknown source (~6300)				
LNA 100	0.86	**0.93**	MTR 146[b]	0.83	0.83	0.85	0.70

	EW0408-40JC Unit A (10.29 mbsf) (>12,800)	Unit B (9.80 mbsf) (>12,800)	Unit C (9.08 mbsf II)[2] (13154±100)[3]
Lethe tephra (~12,600)[k]	0.81	0.80	0.91

Data sources:
  [a] Fierstein and Hildreth (1992).
  [b] Payne et al. (2008).
  [c] Richter et al. (1995).
  [d] Downes (1985).
  [e] Beget et al. (1992).
  [f] Zoltai (1988).
  [g] Westgate (1977).
  [h] Beget et al. (1991).
  [i] Riehle et al. (1999).
  [j] Child et al. (1998).
  [k] Pinney and Beget (1991).
  [1] Calibrated from AMS date presented in Payne et al. (2008).
  [2] SIMAN analysis did not use MgO data due to high standard deviation.
  [3] Calibrated from AMS dates on MEd tephra presented in Beget and Motyka (1998).

22JC deposit and distal White River Ash deposits collected from eastern central Alaska (Beget et al., 1992) has a calculated similarity coefficient of 0.94, clearly indicating the presence of the White River Ash within EW0408-22JC.

EW0408-33JC at 12.78 mbsf

The SIMAN analyses of the full EW0408 tephra dataset presented in this article classified the two cryptotephras from EW0408-33JC at 12.78 and 16.18 mbsf, and the sample at 6.46 mbsf (I) in EW0408-47JC, all as Unit A (Table 3). As described earlier, Unit A has a very high similarity coefficient with rhyolites from the MEVF (>0.96; Table 4). Other mid-Holocene eruptions do not appear to share similarly high values (Table 5). Of the tephra deposits examined in this article, the strongest non-MEVF relationship for all three of the mid-Holocene EW0408 samples is with ECR 162 of Payne et al. (2008), which is chronologically constrained by an underlying *Sphagnum* moss fragment radiocarbon dated by AMS to between 5030–5300 cal yr BP. Despite a similar age with an eruption at Black Peak on the Alaska Peninsula (Miller and Smith, 1987), Payne et al. found little geochemical similarity between ECR 162 and the Black Peak tephra (Riehle et al., 1999); likewise, a low similarity coefficient is calculated for the potentially contemporaneous EW0408-33JC cryptotephra at 12.78 mbsf (Table 5). Payne et al. instead attributed ECR 162 to a previously unidentified Aniakchak eruption that is significantly older than the large caldera-forming eruption at 3400 cal yr BP (Beget et al., 1992).

The chronology of core EW0408-33JC places the date of deposition of the 12.18 mbsf cryptotephra at ~5300 cal yr BP, which is equivalent to the age associated with ECR 162 of Payne et al. (2008). The geochemical composition of these two cryptotephra units bears some overlap (Fig. 8B). However, the 12.18 mbsf tephra in EW0408-33JC appears more closely related to the rhyolitic activity from the MEVF than either ECR 162 or its purported source at Aniakchak on the Alaska Peninsula. Nevertheless, Aniakchak is known to have had at least 40 Holocene eruptions, with at least half of these occurring between 3500 and 10,000 yr ago (Riehle et al., 1999; Neal et al., 2001). It is difficult to disregard Aniakchak as a distal source particularly since it plots in the region of overlap between the EW0408-33JC 12.78 mbsf tephra and ECR 162 in a ternary K_2O-CaO-Fe_2O_3 diagram (Fig. 8B). Conversely, the strong geochemical relationship between the MEVF and the -33JC tephra suggests the likelihood of a mid-Holocene eruption of Mt. Edgecumbe. This observation is supported by independent age dating of bulk peat deposits by Riehle and Brew (1984) that bracket a rhyolitic tephra horizon between 4000–4300 ^{14}C yr BP (4800–5300 cal yr BP; Fig. 2) recovered on the western slope of Mt. Edgecumbe proper.

EW0408-33JC at 16.18 mbsf and EW0408-47JC at 6.46 mbsf (I)

The cryptotephras in cores EW0408-47JC and EW0408-33JC at 6.46 mbsf (I) and 16.18 mbsf, respectively [referred to as the -47JC and -33JC tephras for brevity in the following section], show several equivalent characteristics. The -33JC tephra is well-constrained chronologically by a wood macrofossil only 18 cm above the tephra that was
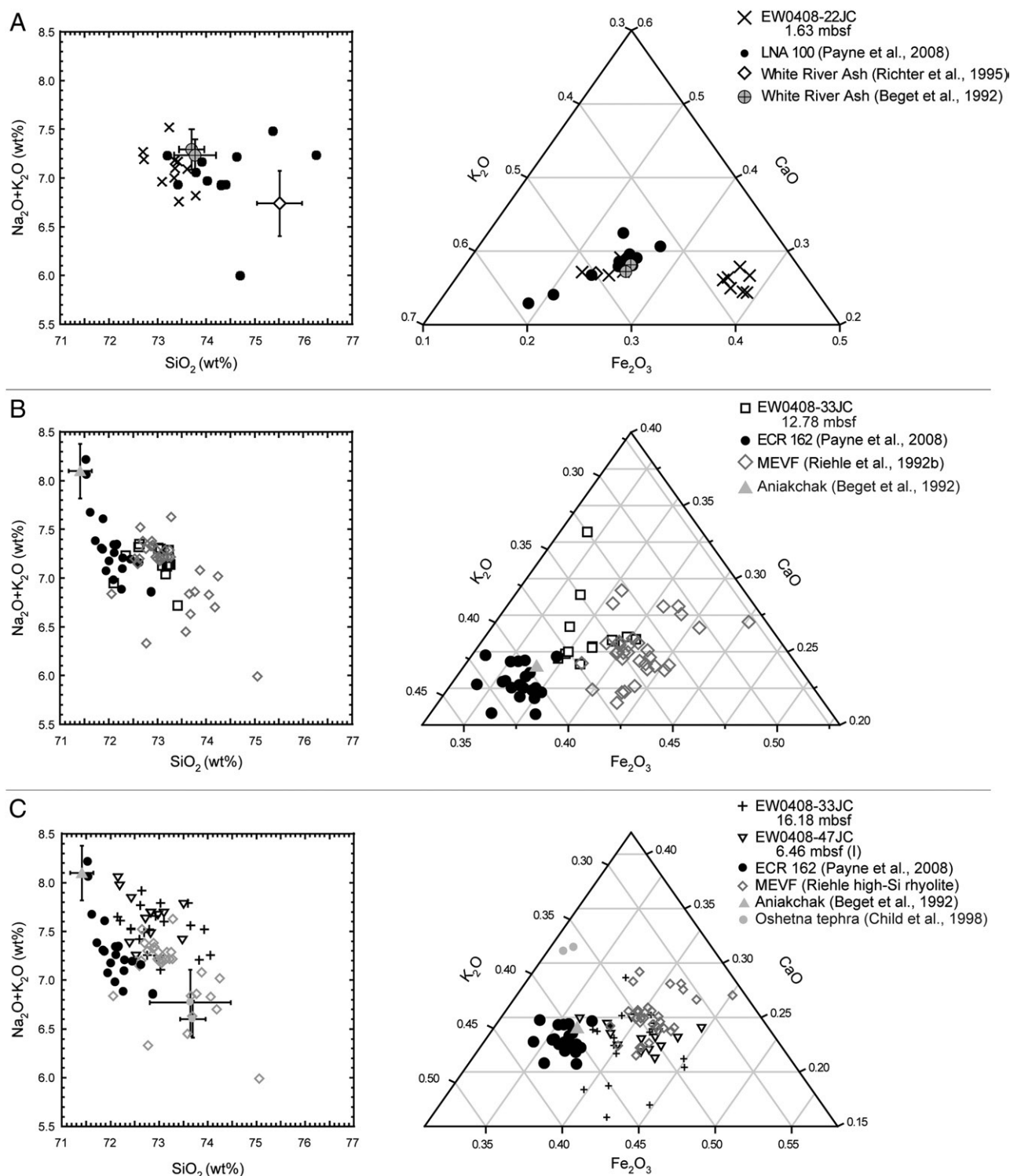
Figure 8. TAS and ternary oxide variation diagrams for EW0408 tephra deposits and regionally significant tephra deposits. (A) The composition of the cryptotephra from core EW0408-22JC appears similar to LNA 100, a cryptotephra from a peat deposit near Juneau, Alaska, that has been linked to the White River Ash. (B) Some compositional overlap exists between the cryptotephra at 12.78 mbsf in core EW0408-33JC and ECR 162; ECR 162 is compositionally similar to the 3400 cal yr BP eruption of Aniakchak (Beget et al., 1992), whereas EW0408-33JC at 12.78 mbsf bears similarities to MEVF activity. (C) The cryptotephras in cores EW0408-33JC (at 16.18 mbsf) and -47JC (at 6.46 msbsf [I]) are compositionally identical and overlap somewhat with ECR 162, which has been attributed to a previously unidentified Aniakchak eruption by Payne et al. (2008). However, both cryptotephras in -33JC and -47JC more closely resemble rhyolitic deposits associated with MEVF activity. Error bars (where shown) indicate 1σ standard deviation of published population means where individual glass analyses were unavailable.

AMS radiocarbon dated to between 6659–6743 cal yr BP (Fig. 4). Although the -47JC tephra has no upper bounding date, it is underlain by a wood fragment between 7501–7608 cal yr BP that is 82 cm below the tephra. The interpolated dates for both tephras using the age models plotted in Fig. 4 place the -33JC tephra at ~6800 cal yr BP, and the -47JC

tephra at ~7300 cal yr BP, a difference of only 500 yr, which may be sufficiently explained by errors in the age models of the two different cores (Telford et al., 2004).

The geochemical characteristics of both the -33JC and -47JC tephras are also comparable. Oxide variation diagrams show both
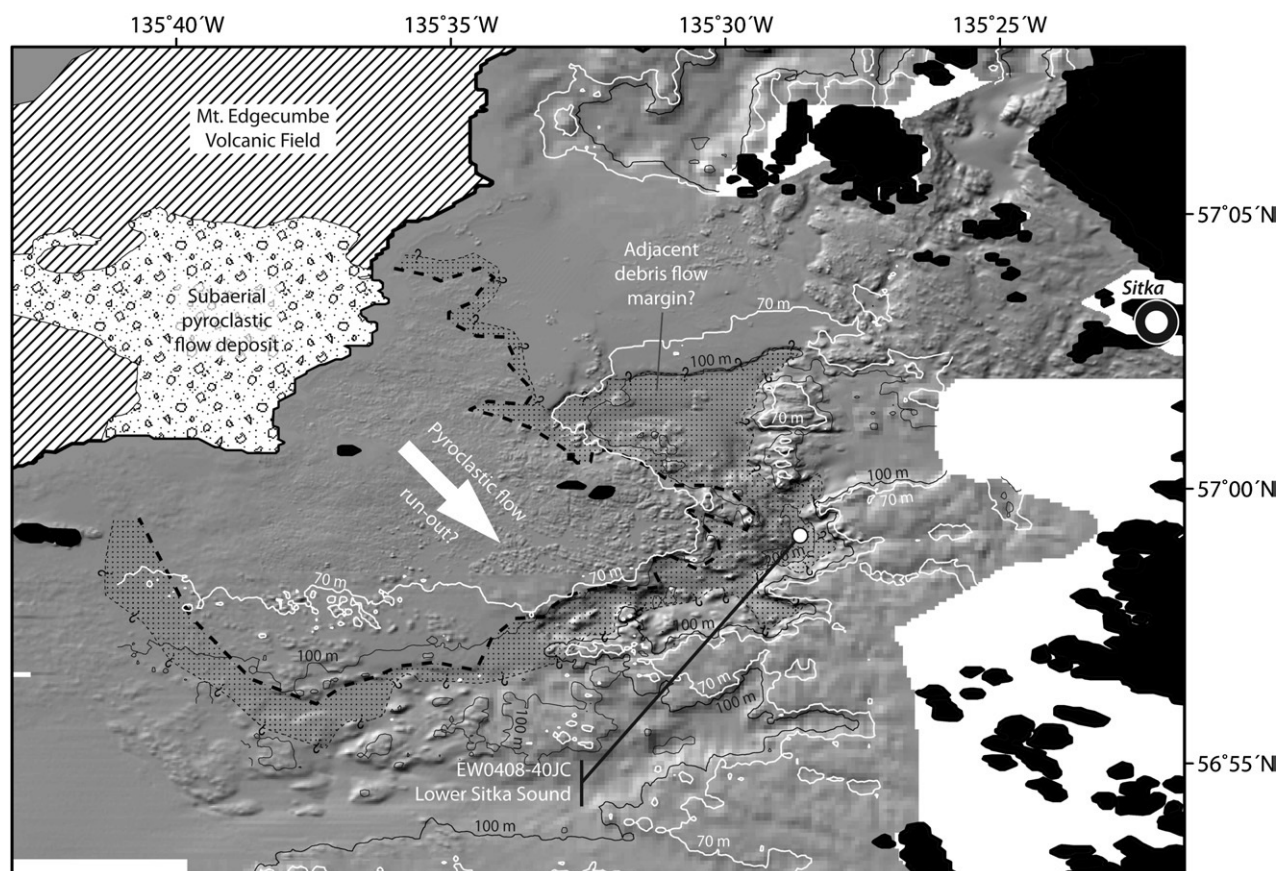
Figure 9. Bathymetry of Sitka Sound in relation to mapped subaerial pyroclastic flows from the MEVF (Riehle et al., 1989). The geometry of the lobe, as well as the sedimentology of EW0408-40JC, suggests that this may be the submerged run-out of the adjacent subaerial flow. White contour line at 70-m water depth indicates eustatic sea level at the time of deposition of the MEd tephra (Fairbanks, 1989).

tephra populations overlapping (Fig. 8C). The multivariate SIMAN analysis calculated a similarity coefficient of 0.99 (Table 3), indicating that the two tephras are virtually identical, and belong to the Unit A designation for the EW0408 tephra suite.

As stated earlier, Unit A is most likely derived from MEVF rhyolitic activity, and potential alternative sources for the -33JC and -47JC tephras appear unlikely (Table 5). The Oshetna tephra, dated to 6700–7000 cal yr BP, and observed in south–central Alaska (Dixon and Smith, 1990; Child et al., 1998), bears little similarity to either the -33JC or -47JC tephras (Table 5; Fig. 8C). Surprisingly, the best similarity coefficient for -47JC is observed with ECR 162 of Payne et al. (2008), but the -47JC geochemical data suffer from the same problems as noted above for the 12.18 mbsf tephra in EW0408-33JC, in that while ECR 162 is attributed to an undocumented Aniakchak eruption (Payne et al., 2008), the geochemical composition of the -47JC tephra correlates better with an MEVF source (Fig. 8C).

The potential for an MEVF source for both the -33JC and -47JC tephras is further supported by a dated rhyolitic horizon contained within a single dated peat sample of 6400–6700 cal yr BP on the southwest coast of Kruzof Island (Riehle and Brew, 1984). This terrestrial peat date is consistent with the interpolated chronology for the -33JC tephra but is slightly too young for a chronological correlation to the -47JC tephra. If the interpolated age of -47JC is correct, then the occurrence of two explosive MEVF eruptions of identical composition occurring within 500 yr of one another may be a potential alternative explanation.

EW0408-25MC3

The poor age control associated with the EW0408-25MC3 core is problematic for understanding its role in the accumulation of MEVF

pyroclastic material. The 35-cm-long core is composed of (i) an upper 19 cm of olive-green diatomaceous silty clay; (ii) a macroscopic 3-cm-thick sandy rhyolitic tephra (Table 2); and (iii) a lower mottled dark-gray silty clay for the remaining 13 cm of the core. In other EW0408 cores from the Gulf of Alaska continental shelf, the upper contact of the dark-gray silty clay unit occurs approximately 12,000 cal yr BP, with the silty clay unit likely reflecting increased glaciomarine sedimentation during deglaciation (Barron et al., 2009). If the overlying diatomaceous clay is a continuous autochthonous record of Holocene biogenic sedimentation, then the EW0408-25MC3 tephra may be contemporaneous with the Latest Pleistocene eruptions of the MEVF. Indeed, the geochemistry of the EW0408-25MC3 tephra supports an MEVF source because of its high similarity to other MEVF-derived EW0408 tephras described here (Table 3; Fig. 5). Until a comprehensive chronology is developed, the conservative interpretation of the EW0408-25MC3 tephra is that it is derived from MEVF activity that is older than 100 yr BP based on interpretation of excess ^{210}Pb data (Rosen et al., 2005; Walinsky et al., 2009).

EW0408-40JC

Whereas the close proximity of the MEVF to the EW0408-40JC core location makes the MEVF seem the likely source of the pyroclastic material contained within -40JC, other large Late Pleistocene eruptions may have potentially contributed tephra. The Lethe tephra represents one of the most explosive eruptions from the Valley of Ten Thousand Smokes in Katmai National Park, Alaska, and occurred at least 14,300–15,200 cal yrs BP (Pinney and Beget, 1991; Fierstein, 2007). Further dating by Reger et al. (2007) on the Kenai Peninsula also constrains several periods of explosive activity to between 16,300–19,200 cal yr BP. Lethe tephra deposits have been identified in

several locations throughout the Kenai and Alaska Peninsulas with some compositional heterogeneity (Pinney, 1993; Riehle et al., 2008), and because of the possibility of deposition in southeast Alaska, the geochemistry of the 'average' Lethe tephra (Pinney and Beget, 1991) was compared against the EW0408 tephra geochemistries. Of the three EW0408 tephra geochemistries, Unit C is the most similar to the Lethe deposit but only with a similarity coefficient of 0.91 (Table 5). This result suggests little similarity between any of the EW0408 tephras and the Lethe tephra. Therefore, it seems most likely that the tephras recovered from core EW0408-40JC are all derived from the MEVF and not from distal volcanic activity along the Alaska Peninsula.

Implications and volcanic hazards

The complicated stratigraphy of core EW0408-40JC makes interpretation of these tephra units difficult (Fig. 7). With the exception of the sample from 9.08 mbsf, the Unit A samples consistently underlie poorly sorted lithogenic muds and gravels that fine upwards into diatomaceous silty clays. These latter deposits presumably represent the autochthonous biogenic sedimentation regime present in Lower Sitka Sound, whereas the sedimentology of the former deposits suggests emplacement by episodic subaqueous pyroclastic flows (Fisher, 1979). Proximal deposits from turbulent subaerial pyroclastic density currents that enter large water bodies and mix with water may transition into aqueous density currents (Orton, 1996), which are known to include a lowermost massive poorly sorted unit with a sharp basal contact that fines upwards (Cole and DeCelles, 1991). Both of these characteristics are present in the deposits contained within EW0408-40JC, as well as several fine-grained upper units that may represent the atmospheric fallout of volcanic ash. Recent high-resolution bathymetric mapping of Sitka Sound (Fig. 9; National Ocean Service Hydrographic Database) shows a low-angle submarine slope extending from the southeast coastline of Kruzof Island towards the site of EW0408-40JC. Previous mapping by Riehle et al. (1989) indicates subaerial pyroclastic flow deposits adjacent to this submarine slope, suggesting that the low-angle slope may be the submarine expression of the subaerial pyroclastic flow deposits (Fig. 9).

The land–sea configuration of Kruzof Island and Sitka Sound prior to deposition of the MEd tephra is complicated by deglacial changes in both eustatic and relative sea level. The LGM lowstand likely exposed a large subaerial region of the shallow margin of Kruzof Island and portions of Sitka Sound. Radiocarbon constraints on the MEd tephra correspond to a eustatic sea level at least 70 m lower than that of today (Fairbanks, 1989). Modern Sitka Sound bathymetric features include an outer sill at approximately 130-m water depth, and the EW0408-40JC core was recovered from an inner basin at 216-m water depth. The presence of freshwater lacustrine diatoms within the laminated siliceous muds (Starratt, S.W., personal communication, 2009) intercalated between the tephra deposits below 9 mbsf in EW0408-40JC (Fig. 3A) argues for the closing of Sitka Sound from the open Gulf of Alaska sometime during the LGM/Holocene deglacial transition. The lack of submerged well-defined cut marine terraces within Sitka Sound (Fig. 9) implies that the major topographic barrier to the Gulf of Alaska was likely the outer sill, and would thus require some amount of vertical adjustment to isolate Sitka Sound. These constraints suggest that the pre-MEd pyroclastic flows from the MEVF crossed the then–exposed margin of Kruzof Island and were deposited within "paleolake" Sitka Sound, which was then subsequently inundated by marine waters. Additional AMS ^{14}C dating and diatom biostratigraphy of EW0408-40JC is underway to better constrain the timing of this inundation.

The tephra stratigraphy of EW0408-40JC is complicated by the consistent presence of the Unit B tephras within, or directly overlying, the poorly sorted mud and gravel units. If these poorly sorted units are preserved portions of two different pyroclastic flow deposits, then possibly the Unit A tephras represent the early-stage eruptive products, whereas the Unit B tephras occurred later in the eruption

sequence. This explanation is consistent with the MEVF originating from a stratified magma chamber (Riehle et al., 1992a).

Subaqueous emplacement of large subaerial pyroclastic flows represents a significant risk in terms of tsunami generation. Although direct displacement of water by the entrance of a pyroclastic flow into the sea is known to generate tsunami waves (e.g., Beget et al., 2008), experimental evidence has also shown that flows at >250°C that encounter bodies of water are also able to generate tsumani via steam explosions (Freundt, 2003). Regardless of the mechanism, tsunamis generated by pyroclastic flows have caused massive loss of life in many regions, including the AD 1883 Krakatau eruption (Carey et al., 2000, 2001) and the Late Bronze Age eruption of Thera on Santorini (McCoy and Heiken, 2000a,b). The close proximity of the city of Sitka to both Kruzof Island and Sitka Sound, combined with the observation that the MEVF has been active several times throughout the Holocene (Riehle and Brew, 1984; Riehle et al., 1992b; this study), suggests that this active volcanic center poses potential future risk to inhabitants and warrants further evaluation for safety considerations.

Conclusions

The marine record of volcanic activity preserved along the Gulf of Alaska margin will prove to be an important component of future Holocene and Late Pleistocene stratigraphic correlations between terrestrial and marine environments in this region. Two examples of such correlations were presented in this article: (i) a Latest Pleistocene MEVF eruption sequence correlation between EW0408-40JC and a nearby lake core from Baranof Island; and (ii) the regionally extensive ~1147 cal yr BP White River Ash deposit. In the case of the White River Ash, this unit has been mapped previously from the Wrangell Volcanic Field eastward into the Canadian Yukon Territory as far as the Great Slave Lake. The discovery of White River Ash in core EW0408-22JC makes this the most southerly Pacific Coast location yet described and implies a much more widespread eruption than previously thought. Corroborating evidence for this southerly dispersal is the presence of White River Ash contained within peat deposits near Juneau, Alaska (Payne et al., 2008).

The MEVF itself has also proven an important source of regional stratigraphic horizons. The MEd dacitic tephra (Engstrom et al., 1990; Beget and Motyka, 1998; Riehle et al., 1992b) already provides a useful regional chronostratigraphic marker, but pyroclastic flow deposits in EW0408-40JC show evidence of at least two major eruptions prior to the deposition of MEd (Fig. 9), agreeing with previous terrestrial survey work (Riehle et al., 1992a,b). The identification of three mid-Holocene MEVF cryptotephras in cores EW0408-33JC and -47JC argue for the presence of additional stratigraphic markers in the adjacent terrestrial environment. It is important to note, however, that the limited range of MEVF rhyolitic major-element compositions will not make stratigraphic correlations between sites easy and straightforward, particularly if no chronological information is available.

References

Barron, J.A., Bukry, D., Dean, W.E., Addison, J.A., Finney, B.P., 2009. Paleoceanography of the Gulf of Alaska during the past 15,000 years: results from diatoms, silicoflagellates, and geochemistry. Marine Micropaleontology 72, 176–195.

Beget, J.E., Keskinen, M.J., 2003. Trace-element geochemistry of individual glass shards of the Old Crow tephra and the age of the Delta glaciation, central Alaska. Quaternary Research 60, 63–69.

Beget, J.E., Motyka, R.J., 1998. New dates on late Pleistocene dacitic tephra from the Mount Edgecumbe volcanic field, southeastern Alaska. Quaternary Research 49, 123–125.

Beget, J.E., Mason, O., Anderson, P., 1992. Age, extent and climatic significance of the c. 3400 BP Aniakchak tephra, western Alaska, USA. Holocene 2, 51–56.

Beget, J.E., Stihler, S.D., Stone, D.B., 1994. A 500-year-long record of tephra falls from Redoubt volcano and other volcanos in Upper Cook Inlet, Alaska. Journal of Volcanology and Geothermal Research 62, 55–67.

Beget, J., Gardner, C., Davis, K., 2008. Volcanic tsunamis and prehistoric cultural transitions in Cook Inlet, Alaska. Journal of Volcanology and Geothermal Research 176, 377–386.

Blockley, S.P.E., Pyne-O'Donnell, S.D.F., Lowe, J.J., Matthews, I.P., Stone, A., Pollard, A.M., Turney, C.S.M., Molyneux, E.G., 2005. A new and less destructive laboratory procedure for the physical separation of distal glass tephra shards from sediments. Quaternary Science Reviews 24, 1952–1960.

Borchardt, G.A., 1974. The SIMAN coefficient for similarity analysis. Classification Society Bulletin 3, 2–8.

Borchardt, G.A., Aruscavage, P.J., Millard Jr., H.T., 1972. Correlation of the Bishop Ash, a Pleistocene marker bed, using instrumental neutron activation analysis. Journal of Sedimentary Petrology 42, 301–306.

Carey, S., Sigurdsson, H., Mandeville, C.W., Bronto, S., 2000. Volcanic hazards from pyroclastic flow discharge into the sea: examples from the 1883 eruption of Krakatau, Indonesia. In: McCoy, F.W., Heiken, G. (Eds.), Volcanic Hazards and Disasters in Human Antiquity. Geological Society of America, Boulder, CO, pp. 1–14.

Carey, S., Morelli, D., Sigurdsson, H., Bronto, S., 2001. Tsunami deposits from major explosive eruptions: an example from the 1883 eruption of Krakatau. Geology 29, 347–350.

Child, J.K., Beget, J.E., Werner, A., 1998. Three Holocene tephras identified in lacustrine sediment cores from the Wonder Lake area, Denali National Park and Preserve, Alaska, USA. Arctic and Alpine Research 30, 89–95.

Clague, J.J., Evans, S.G., Rampton, V.N., Woodsworth, G.J., 1995. Improved age estimates for the White River and Bridge River tephras, western Canada. Canadian Journal of Earth Sciences 32, 1172–1179.

Cole, R.B., DeCelles, P.G., 1991. Subaerial to submarine transitions in early Miocene pyroclastic flow deposits, southern San Joaquin basin, California. Geological Society of America Bulletin 103, 221–235.

Davies, S.M., Hoek, W.Z., Bohncke, S.J.P., Lowe, J.J., O'Donnell, S.P., Turney, C.S.M., 2005. Detection of Lateglacial distal tephra layers in the Netherlands. Boreas 34, 123–135.

Dixon, E.J., Smith, G.S., 1990. A regional application of tephrochronology in Alaska. In: Lasca, N.P., Donahue, J. (Eds.), Archaeological Geology of North America. Geological Society of America, Boulder, CO, pp. 383–398.

Downes, H., 1985. Evidence for magma heterogeneity in the White River Ash (Yukon Territory). Canadian Journal of Earth Sciences 22, 929–934.

Eberlein, G.D., Churkin Jr., M., 1970. Tlevak Basalt, west coast of Prince of Wales Island, southeastern Alaska. In: Cohee, G.V., Bates, R.G., Wright, W.B. (Eds.), Changes in stratigraphic nomenclature by the U.S. Geological Survey, 1968. Geological Survey Bulletin 1294-A. United States Government Printing Office, Washington D.C, pp. 25–55.

Engstrom, D.R., Hansen, B.C.S., Wright, H.E., 1990. A possible Younger Dryas record in southeastern Alaska. Science 250, 1383–1385.

Fairbanks, R.G., 1989. A 17,000-year glacio-eustatic sea-level record—influence of glacial melting rates on the Younger Dryas event and deep-ocean circulation. Nature 342, 637–642.

Fierstein, J., 2007. Explosive eruptive record in the Katmai region, Alaska Peninsula: an overview. Bulletin of Volcanology 69, 469–509.

Fisher, R.V., 1979. Models for pyroclastic surges and pyroclastic flows. Journal of Volcanology and Geothermal Research 6, 305–318.

Fisher, D.A., Wake, C.P., Kreutz, K., Yalcin, K., Steig, E.J., Mayewski, P.A., Anderson, L., Zheng, J., Rupper, S., Zdanowicz, C., Demuth, M., Waszkiewicz, M., Dahl-Jensen, D., Goto-Azuma, K., Bourgeois, J.B., Koerner, R., Sekerka, J., Osterberg, E.C., Abbott, M.B., Finney, B., Burns, S.J., 2004. Stable isotope records from Mt. Logan, Eclipse ice cores and nearby Jellybean Lake; water cycle of the North Pacific over 2000 years and over five vertical kilometers; sudden shifts and tropical connections. Geographie Physique et Quaternaire 58, 337–352.

Freundt, A., 2003. Entrance of hot pyroclastic flows into the sea: experimental observations. Bulletin of Volcanology 65, 144–164.

Goldstein, J., Newbury, D.E., Joy, D.C., Lyman, C.E., Echlin, P., Lifshin, E., Sawyer, L.C., Michael, J.R., 2003. Scanning Electron Microscopy and X-ray Microanalysis. Springer Science + Business Media, Inc., New York.

Greene, H.G., O'Connell, V.M., Wakefield, W.W., Brylinsky, C.K., 2007. The offshore Edgecumbe lava field, southeast Alaska: geologic and habitat characterization of a commercial fishing ground. In: Todd, B.J., Greene, H.G. (Eds.), Mapping the Seafloor for Habitat Characterization. Geological Association of Canada, pp. 277–295.

Grewingk, C., 1850. Geology of Alaska and the Northwest Coast of America. The University of Alaska Press, Fairbanks, AK.

Haberle, S.G., Lumley, S.H., 1998. Age and origin of tephras recorded in postglacial lake sediments to the west of the southern Andes, 44°S to 47°S. Journal of Volcanology and Geothermal Research 84, 239–256.

Hillenbrand, C.D., Moreton, S.G., Caburlotto, A., Pudsey, C.J., Lucchi, R.G., Smellie, J.L., Benetti, S., Grobe, H., Hunt, J.B., Larter, R.D., 2008. Volcanic time-markers for Marine Isotopic Stages 6 and 5 in Southern Ocean sediments and Antarctic ice cores: implications for tephra correlations between palaeoclimatic records. Quaternary Science Reviews 27, 518–540.

Le Bas, M.J., Lemaitre, R.W., Streckeisen, A., Zanettin, B., 1986. A chemical classification of volcanic rocks based on the total alkali silica diagram. Journal of Petrology 27, 745–750.

Lerbekmo, J.F., 2008. The White River Ash: largest Holocene Plinian tephra. Canadian Journal of Earth Sciences 45, 693–700.

Lowe, D.J., 2008. Globalization of tephrochronology: new views from Australasia. Progress in Physical Geography 32, 311–336.

Mashiotta, T.A., Thompson, L.G., Davis, M.E., 2004. The White River Ash: new evidence from the Bona-Churchill ice core record. Eos Trans. AGU 85 Fall Meet. Suppl., Abstract PP21A-1369.

McCoy, F.W., Heiken, G., 2000a. The Late-Bronze Age explosive eruption of Thera (Santorini), Greece: regional and local effects. In: McCoy, F.W., Heiken, G. (Eds.), Volcanic Hazards and Disasters in Human Antiquity. Geological Society of America, Boulder, CO, pp. 43–70.

McCoy, F.W., Heiken, G., 2000b. Tsunami generated by the Late Bronze Age eruption of Thera (Santorini). Greece. Pure and Applied Geophysics 157, 1227–1256.

Miller, T.P., Smith, R.L., 1987. Late Quaternary caldera-forming eruptions in the eastern Aleutian arc, Alaska. Geology 15, 434–438.

Neal, C.A., McGimsey, R.G., Miller, T.P., Riehle, J.R., Waythomas, C.F., 2001. Preliminary volcano-hazard assessment for Aniakchak Volcano, Alaska. In: US Geological Survey (Ed.), Open-File Report 00-519. Alaska Volcano Observatory, Anchorage, Alaska, p. 42.

Orton, G.J., 1996. Volcanic environments. In: Reading, H.G. (Ed.), Sedimentary environments: processes, facies, and stratigraphy. Blackwell Science, Oxford, pp. 485–567.

Payne, R., Blackford, J., 2004. Distal tephra deposits in southeast Alaskan peatlands. In: Emond, D., Lewis, L. (Eds.), Yukon Exploration and Geology 2003. Whitehorse, Canada, Yukon Geological Survey, pp. 191–197.

Payne, R., Blackford, J., van der Plicht, J., 2008. Using cryptotephras to extend regional tephrochronologies: an example from southeast Alaska and implications for hazard assessment. Quaternary Research 69, 42–55.

Pearce, N.J.G., Bendall, C.A., Westgate, J.A., 2008. Comment on "Some numerical considerations in the geochemical analysis of distal microtephra" by A.M. Pollard, S. P.E. Blockley and C.S. Lane. Applied Geochemistry 23, 1353–1364.

Pinney, D. S. (1993). "Late Quaternary glacial and volcanic stratigraphy near Windy Creek, Katmai National Park, Alaska." Unpublished M.S. thesis, University of Alaska Fairbanks.

Pinney, D.S., Beget, J.E., 1991. Late Pleistocene volcanic deposits near the Valley of Ten Thousand Smokes, Katmai National Park, Alaska. In: Reger, R.D. (Ed.), Short Notes on Alaskan Geology 1991. State of Alaska, Division of Geological and Geophysical Surveys, Anchorage, AK, pp. 45–54.

Pollard, A.M., Blockley, S.P.E., Lane, C.S., 2006. Some numerical considerations in the geochemical analysis of distal microtephra. Applied Geochemistry 21, 1692–1714.

Reger, R.D., Sturmann, A.G., Berg, E.E., Burns, P.A.C., 2007. A guide to the Late Quaternary history of northern and western Kenai Peninsula, Alaska. State of Alaska Dept. of Natural Resources, Division of Geological and Geophysical Surveys, Fairbanks, Alaska, p. 120.

Reimer, P.J., Baillie, M.G.L., Bard, E., Bayliss, A., Beck, J.W., Bertrand, C.J.H., Blackwell, P.G., Buck, C.E., Burr, G.S., Cutler, K.B., Damon, P.E., Edwards, R.L., Fairbanks, R.G., Friedrich, M., Guilderson, T.P., Hogg, A.G., Hughen, K.A., Kromer, B., McCormac, G., Manning, S., Ramsey, C.B., Reimer, R.W., Remmele, S., Southon, J.R., Stuiver, M., Talamo, S., Taylor, F.W., van der Plicht, J., Weyhenmeyer, C.E., 2004. IntCal04 terrestrial radiocarbon age calibration, 0–26 cal kyr BP. Radiocarbon 46, 1029–1058.

Riehle, J.R., Brew, D.A., 1984. Explosive latest Pleistocene(?) and Holocene activity of the Mount Edgecumbe volcanic field, Alaska. In: Reed, K.M., Bartsch-Winkler, S. (Eds.), The United States Geological Survey in Alaska: accomplishments during 1982, pp. 111–115.

Riehle, J.R., Brew, D.A., Lanphere, M.A., 1989. Geologic map of the Mount Edgecumbe volcanic field, Kruzof Island, southeastern Alaska. Miscellaneous Investigations Series Map I 1983. U.S. Geological Survey.

Riehle, J.R., Champion, D.E., Brew, D.A., Lanphere, M.A., 1992a. Pyroclastic deposits of the Mount Edgecumbe volcanic field, southeast Alaska: eruptions of a stratified magma chamber. Journal of Volcanology and Geothermal Research 53, 117–143.

Riehle, J.R., Mann, D.H., Peteet, D.M., Engstrom, D.R., Brew, D.A., Meyer, C.E., 1992b. The Mount Edgecumbe tephra deposits, a marker horizon in southeastern Alaska near the Pleistocene Holocene boundary. Quaternary Research 37, 183–202.

Richter, D.H., Preece, S.J., McGimsey, R.G., Westgate, J.A., 1995. Mount Churchill, Alaska: source of the late Holocene White River Ash. Canadian Journal of Earth Sciences 32, 741–748.

Riehle, J. R., Meyer, C. E., and Miyaoka, R. T. (1999). Data on Holocene tephra (volcanic ash) deposits in the Alaska Peninsula and lower Cook Inlet region of the Aleutian volcanic arc, Alaska. USGS Open-File Report 99-135.

Riehle, J.R., Ager, T.A., Reger, R.D., Pinney, D.S., Kaufman, D.S., 2008. Stratigraphic and compositional complexities of the late Quaternary Lethe tephra in South-central Alaska. Quaternary International 178, 210–228.

Robinson, S.D., 2001. Extending the late Holocene White River ash distribution, northwestern Canada. Arctic 54, 157–161.

Rosen, G.P., Jaeger, J.M., Stoner, J.S., Channell, J.E.T., 2005. Establishing the temporal resolution of high-latitude paleoclimatic and paleomagnetic signals in bioturbated Gulf of Alaska continental margin sediments. Eos Trans AGU 86 abstract H51G-0446.

Shane, P., Nairn, I.A., Martin, S.B., Smith, V.C., 2008. Compositional heterogeneity in tephra deposits resulting from the eruption of multiple magma bodies: Implications for tephrochronology. Quaternary International 178, 44–53.

Shipboard Science Party, 1993. Site 887. In: Rea, D.K., Basov, I.A., Janecek, T.R., Palmer-Julson, A., et al. (Eds.), Proceedings of the Ocean Drilling Program, Initial Reports. Ocean Drilling Program, College Station, TX, pp. 335–391.

Sikes, E.L., Samson, C.R., Guilderson, T.P., Howard, W.R., 2000. Old radiocarbon ages in the southwest Pacific Ocean during the last glacial period and deglaciation. Nature 405, 555–559.

Stoner, J.S., Jennings, A., Kristjansdottir, G.B., Dunhill, G., Andrews, J.T., Hardardottir, J., 2007. A paleomagnetic approach toward refining Holocene radiocarbon-based chronologies: paleoceanographic records from the north Iceland (MD99-2269) and east Greenland (MD99-2322) margins. Paleoceanography 22. doi10.1029/2006PA001285.

Stuiver, M., Reimer, P.J., 1993. Extended ^{14}C data base and revised CALIB 3.0 radiocarbon age calibration program. Radiocarbon 35, 137–189.

Telford, R.J., Heegaard, E., Birks, H.J.B., 2004. All age–depth models are wrong: but how badly? Quaternary Science Reviews 23, 1–5.

Turney, C.S.M., Harkness, D.D., Lowe, J.J., 1997. The use of microtephra horizons to correlate late-glacial lake sediment successions in Scotland. Journal of Quaternary Science 12, 525–531.

Walinsky, S.E., Prahl, F.G., Mix, A.C., Finney, B.P., Jaeger, J.M., Rosen, G.P., 2009. Distribution and composition of organic matter in surface sediments of coastal southeast Alaska. Continental Shelf Research 29, 1565–1579.